Mediterranean Archaeology and Archaeometry
2024, 24(3), 1131
ISSN:2241-8121
https://www.maajournal.com/ **Research Article**

Mineralogical and Thermal Analysis of Ancient Ceramic Artifacts Based on Modern Techniques of Ceramic Studies

Md Saifur Rahman [1], Hendrik Simon Cornelis Metselaar [1,2*], Bushroa Binti Abdul Razak [1,3]

[1] MSc, Department of Mechanical Engineering, Faculty of Engineering, Universiti Malaya, Kuala Lumpur, Malaysia
[2] Associate Professor, Centre of Advanced Materials, Faculty of Engineering, Universiti Malaya, Kuala Lumpur, Malaysia
[3] Professor, Centre of Advanced Manufacturing and Material Processing, Faculty of Engineering, Universiti Malaya, Kuala Lumpur, Malaysia
* **Corresponding Author:** h.metselaar@um.edu.my

Citation: Rahman, M. S., Metselaar, H. S. C., & Razak, B. B. A. (2024). Mineralogical and Thermal Analysis of Ancient Ceramic Artifacts Based on Modern Techniques of Ceramic Studies. *Mediterranean Archaeology and Archaeometry, 24*(3), 38–56. 10.5281/zenodo.13383260

ARTICLE INFO

Received: 14 Aug 2023
Accepted: 22 Dec 2023

ABSTRACT

In this study, the mineralogical and thermal behavior of the two ceramic sherds from the Museum of Asian Art (MoAA), Universiti Malaya (One sherd of blue-white underglaze porcelain from Jingdezhen and one of sherd reddish-brown earthenware from North Sumatra) was analysed through chemical analyses, spectroscopic, mineralogical, and thermal analyses. Traditional attribution is typically done through visual identification by professional archaeologists. Modern material characterization methods, such as thermal analysis, density measurement, Fourier Transform Infrared Spectroscopy (FTIR), X-Ray Diffraction (XRD), Thermomechanical Analysis (TMA), and X-Ray Fluorescence Spectrometry (XRF), can help identify material origins and manufacturing locations. The chemical analyses results by XRF indicate most abundant is SiO2 and the most abundant mineral is quartz investigated by X-ray diffraction (XRD). Based on X-ray diffraction (XRD) and Fourier Transform Infrared Spectroscopy, firing temperature ranges can be determined as 700-1050°C. Low-temperature mineral phases like calcite, muscovite, and quartz were observed in both sherds. Diopside develops with increasing firing at high temperatures above 850 °C. Gehlenite is the predominant new mineral at 900 °C and anorthite forms at between 1000-1050 °C which distinguished between two sherds. Thermomechanical Analysis (TMA) indicates the deformation temperature of earthenware and porcelain sherd are 824 °C and 1000 °C respectively. The earthenware sherd shows higher total shrinkage (9.90%) than porcelain sherd (11.68%). Differential Thermal Analysis (DTMA) showed mullite formation between 1150-1400 °C. Combining traditional and modern approaches is essential for the identification of ceramic artifacts.

Keywords: Artifact, FTIR, TMA, XRD, XRF.

INTRODUCTION

Pottery and ceramic artifacts are highly regarded archaeological relics due to their status as the first synthetic materials developed by human hands with creativity (Sciau & Goudeau, 2015). Clay, a primary raw material in ceramic goods, provides plasticity and body shape, making earthenware tiles and clay-based ceramics and tiles burned below 1100°C (Pradell & Molera, 2020). Researchers identified ceramics that involved the exchange of Southeast Asian earthenware and stoneware ceramics between the ninth and sixteenth centuries AD (Ueda et al. 2017). The exact chemistry and mineral composition determine the thermal characteristics, color, refractoriness, and mechanical strength after firing (El Idrissi et al., 2018). Ceramics contain various chemical components of crystalline and amorphous phases depending on the modification and transformation of raw materials at different processing conditions (Lara, 2020). Ceramics are produced in different areas by different manufacturing systems, techniques, and compositions. The basic compendia on ceramics artifacts consider various techniques of manufacturing systems with parameters (Chenoweth & Farahani, 2015). The design, ornamentation, and manufacturing processes provide information about the lifestyle and culture of one ancestor (Kazakou, Zorba,

Vourlias, Pavlidou, & Chrissafis, 2019; Baziotis, Xydous, Manimanaki, & Liritzis, 2020). Ceramic research in archaeology aids in reconstructing historical human activities, particularly production techniques, which can reveal social, economic, and political aspects of societies (El Ouahabi, El Idrissi, Daoudi, El Halim, & Fagel, 2019).

Natural porcelain stone is a type of rock that may be found in the southern region of China. It contains quartz, fine-particle hydro-muscovite, and small amounts of feldspar and kaolinite (Pradell & Molera, 2020; Tite, Freestone & Wood, 2012). The technological developments in Jingdezhen and the rest of China are crucial research topics (Wu et al., 2020). The invention of glaze, spanning from Tang Dynasty technical glaze stoneware to Yuan and Ming Dynasty blue-and-white porcelain, significantly advanced porcelain technology (Wu et al., 2020). Southeast Asian-Chinese kilns produced ornamental and architectural finishing porcelain, underglaze blue designs, and functional ceramic dishes and bowls with cobalt blue under-glaze and overglaze polychrome enamel motifs (Lim, 2018). The slow-wheel method is necessary to create jars with everted rims, which are typical of most of the local pottery (Rangkuti & Fauzi, 2019). Ceramic bodies with prolonged burial, interacting with Ca-rich fluids and secondary calcite formation, typically have greater Ca contents towards the surface (Osticioli et al., 2012). Blue and white porcelain ceramic fragments date to the early 14th century CE, with Jingdezhen Kiln believed to have created pottery since the early Ming Dynasty (Husni et al., 2019). The Pa-O kiln in Southern Asia is known for its high-fired earthenware, characterized by clay with a high sand content.

Archaeometric studies assess manufacturing processes, providing insights into ancient societies' territorial exploitation during historic and prehistoric periods (Liritzis et al., 2020). Ancient ceramics can be identified using expert visual and science and technology approaches, with expert professionals providing recognition and judgment, and standard databases for corporate settings (Mu et al., 2019). Though ceramic technology is the oldest human tradition, scientific knowledge has only developed recently (Emami et al., 2016). It is therefore proposed that traditional typology in the study of ceramic artifacts can be combined with modern materials characterization methods (Enyuan et al., 2021). Scientific and technical archaeology uses advanced technologies to identify ancient pottery's compositional and structural roots, using chemical composition, petrographic analyses, and visual inspection (Enyuan et al., 2021; Velraj et al., 2010; Javanshah, 2018). Analytical techniques like FTIR, XRD, Raman Spectroscopy, and TMA are widely used for studying ancient ceramic processes, historical production sites, and trade routes (Velraj et al., 2010; Osticioli et al., 2012; Xanthopoulou, Iliopoulos, & Liritzis, 2020; Panagopoulou et al., 2018). Investigations for authentication should focus on long-term interaction between objects and environments, resulting in unique compositional and microstructural characteristics absent in modern imitations (Osticioli et al., 2012).

Southeast Asia played a crucial role in the global trade network that connected societies from the Mediterranean region to Han China, as well as with China and, to a limited extent, Japan (Colomban, Kırmızı, & Simsek Francil, 2021). At the start of the sixteenth century, direct maritime trade routes between the Indian Ocean and the Mediterranean were developed, allowing for the discovery of the oldest Chinese porcelain and celadon found in Europe dating to the ninth to eleventh centuries AD. However, it appears that the dispersion of Chinese pottery in the western end of the Mediterranean was driven by other circumstances, rather than by the development of international trade networks in the tenth century (Gutiérrez et al., 2021; Oulmakki et al., 2023). The organisation of the global trading system was evident from recent archaeological discoveries and historical literary narratives, as they involved several land and sea trading routes connecting the Mediterranean and South Asia, as well as extending eastward to China and Southeast Asia (Sing Chew, 2015). The Chinese ceramics, created by potters, comprised a variety of glazed and unglazed earthenware sherds. They documented the beginnings of a vast "globalized" maritime trading network that linked the late prehistoric region to cultures and polities in South Asia, China, and the Mediterranean region (Lim, 2018). Increasing accessibility and connectivity between Asia and the Mediterranean is being achieved in part through the development of a global investment network of maritime infrastructures. Though not consistently, there has been a notable growth in connectivity between China and the Mediterranean region (Oulmakki et al., 2023).

Southeast Asia served as the focal point for the expansion of trans-Asian trade and commerce (Ueda et al., 2017). Fine paste ware (FPW) is a unique earthenware ceramic found in coastal Southeast Asia, produced between the 11th and 14th centuries CE. Found in modern-day Thailand, Malaysia, Singapore, and Indonesia (Jutimoosik et al., 2017; Tai et al., 2020). Chinese porcelain, produced at the Jingdezhen kiln site, reached perfection during the Song, Ming, and Qing dynasties. Techniques for polychrome underglaze and overglaze painting advanced during the Ming and Qing dynasties (R. B. Heimann and M. Maggetti, 2019). Ancient Chinese porcelain, classified as earthenware and porcelain, can be dated using basic techniques, but faces challenges due to aesthetic preferences and visual characteristics (Dias, Prudêncio, De Matos, & Rodrigues, 2013). Additionally, while firing, they undergo physical and chemical changes that depend not only on their original composition but also on the maximum temperature, the length of time, and the firing environment. As a result, their investigation cannot be adequately supported using only one analytical technique. A combination of analytical processes such as XRF,

Raman Spectroscopy, XRD, and TMA present a comprehensive method for characterizing ceramic artifacts.

The paper's main goal is to establish a connection between the raw materials used to make Chinese porcelain and earthenware bodies from Sumatra. Additionally, chemical compositions, mineral analysis, and observed thermal analysis were used to contribute to the knowledge about the raw materials themselves. From the collections of the Museum of Asian Art, Universiti Malaya, two sherds of well-known blue-white underglaze porcelain and reddish-brown earthenware from Jingdezhen, South China, and Sumatra respectively have been investigated.

METHODOLOGY

Ceramic Sherd Material and Sample Preparation

Two ceramic sherds samples were taken for investigating the ceramic bodies and glaze. The ceramic samples were collected from the Museum of Asian Art (MoAA) for analyzing using material characterization techniques of FTIR, XRD, XRF, and TMA as well as an investigation of the physical properties of ceramic sherds.

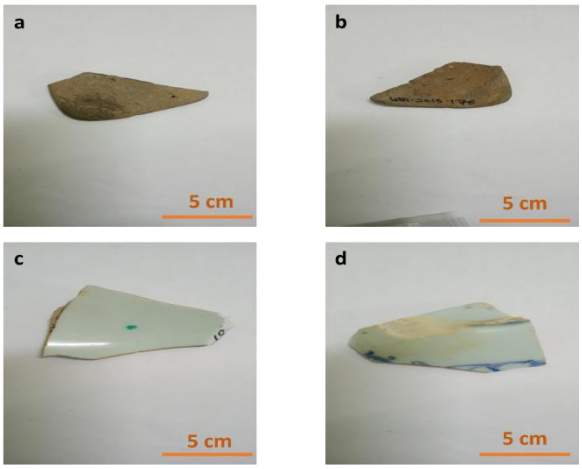

Figure 1. Ceramic Fragments of Sherd 1 (a) Outside (b) Inside and Sherd 2 (c) Outside (d) Inside

Tiny samples from the fragments were cut and milled for preparing a fine powder sample using Ring Crusher for 30 seconds. The powder samples were used for XRD, FTIR, XRF, and a small piece of ceramic cut from ceramic sherds for a solid specimen for the test of TMA. The description of ceramic sherd list in Table 1 and probable site map ishown in Figure 2.

Table 1. Description of Ceramic Sherd Samples Based on Expert Opinions

Sample	Typology							Chronology	
	Part of Vessel	Raw Materials based on Ceramic Type	Glaze Status	Color	Brilliance	Decoration	Technique Used	Period	Origin
Sherd 1	Body of Jar	Earthenware	No Glaze	Reddish Brown	Matt	Inside saturation, porous	Potter's wheel	Ming	Southeast Aisa Sumatra
Sherd 2	Body of Bowl	Porcelain	Glaze (Both Sides)	Blue and white	Glossy	Design motif at outside (underglaze)	Potter's wheel	Ming	South China

Figure 2. Probable Site Map of the Sherd Collection in the Sumatra and Jingdezhen Area

Material Characterization Methods

The density of the sherds was measured by the Archimedes method. FTIR was performed for the study of chemical bonds in the sherds. FTIR was performed on a Bruker Tensor 27 with ATR in the frequency range 400-4000 cm-1. The chemical component analysis was studied using a Benchtop XRF (Supermini200 Wave-length Dispersive X-Ray Fluorescence) with an end-window 4 kW Rh X-ray tube operating at 50 kV and 80 mA (Rix 3100; Rigaku Corp., Akishima, Tokyo, Japan). XRD was done to examine the crystalline structure of ceramic sherds. The X-ray patterns of the powders were obtained using an automated X-ray powder diffractometer (PANalytical X' Pert3) with start and end angles for 2 θ = 5 to 90°. The scan step time was 15 sec/step, step size 0.020, and voltage and current were 45 kV and 40 mA respectively. The analysis was performed by the Profex software (Doebelin and Kleeberg 2015). The thermomechanical analysis was obtained using SETSYS SETARAM (Csáki et al., 2021; Porozova et al., 2013) and AKTS Calisto Processing software was used for analyzing the data.

RESULTS AND DISCUSSION

Chemical Composition Analysis

The chemical study of the main, minor, and trace elements produces a compositional "fingerprint" that can be used to distinguish between groups of pottery manufactured from the same raw materials and to group together pottery made from different raw materials (Tite, 2008). SiO_2 is the most common oxide, followed by Al_2O_3. While the other oxides (TiO_2 and MnO) are present in small amounts, the levels of Fe_2O_3, CaO, K_2O, and MgO are considerable. The reddish-brown color of the mineral kaolinite is caused by the presence of Fe_2O_3, a typical impurity connected to kaolin clay deposits (Abubakar et al., 2020). The ceramic sherd 2 indicates reddish brown color with 5.53% of iron oxide. The chemical composition of sherds are shown in Table 2.

Table 2. Chemical Composition of Ceramic Sherds

Sherd	SiO_2	Al_2O_3	Fe_2O_3	K_2O	MgO	TiO_2	CaO	CoO	References
	%	%	%	%	%	%	%	%	
Sherd 1 Earthenware (Sumatra)	71.8	16.9	5.53	1.78	1.49	1.3	0.14	0.034	This study
Sherd 2 Porcelain (Jingdezhen)	73.1	16.2	2.78	4.57	0.077	0.11	2.43	0.021	This study
Kota Cina North Sumatra Earthenware	69.31	20.02	4.54	1.14	ND	1.13	0.69	ND	(Jutimoosik et al., 2017)
White-Blue Ming Porcelain	74.04	19.58	0.96	3.44	0.21	0.05	0.61	0.83	(Dias et al., 2013; Wen et al., 2019; Simsek et al., 2015)

*ND: Not Detected

The origin of the clay and other elements used to make pottery has a significant impact on its chemical makeup as well as mineralogical analysis. Additionally, changes in trace element concentrations reveal geological diversity. The main elements of earthenware are Al2O3, SiO2, and Fe2O3. The ceramic sherd 1 showed the compositions which indicates the similarities with the Kota Cina in North Sumatra earthenware ceramics with SiO2 (69.31%), Al2O3 (20.02%), K2O (1.14%), TiO2 (1.13%), Fe2O3 (4.54%), MnO (0.10%) (Jutimoosik et al., 2017). The Fe2O3 of ceramic indicates the reddish-brown color of sherd in Figure 1. The higher amounts of SiO2 indicate the large number of quartz minerals which also meet the chemical composition of earthenware of Kota Cina, North Sumatra. The XRD pattern shows a large peak with quartz. K2O acts as a flux at the time of the sintering process (Jutimoosik et al., 2017).

Similarly, the ceramic sherd 2 showed the major and minor chemical composition of SiO2, Al2O3, K2O, TiO2, Fe2O3, and MnO which indicates the similarities with the blue-white porcelain of the Yuan or Ming dynasty of Jingdezhen Royal Kiln, South China (Wu et al., 2020). The blue-and-white porcelain bodies have respective Al2O3, SiO2, and K2O concentrations of 19.12%-21.25, 71.88%-74.26%, and 3.61%-3.74%, which correspond to low aluminium, high silicon, and high potassium, respectively. These characteristics of element composition are also like the blue-and-white porcelains from Jingdezhen in the Ming dynasty when compared with the chemical compositions of porcelains (Wen et al., 2019). Due to the impact of fluxing oxides, the presence of alkaline-rich phase amounts (K2O) in the sintered sample speeds up the vitrification process which indicates for sherd 2 with a higher amount of K2O (4.57%). The amorphous silica released during the breakdown of metakaolin may potentially result in the creation of a vitreous phase. For sherd 1, the lower quantity of K2O (1.78%) because the vitreous phase has not yet developed in these temperatures, the high porosity of the bodies can be explained (Zouaoui & Bouaziz, 2017).

Jinxiu Wen defined a function (F) based on the porcelain compositions that can help to discriminate between porcelains from the Yuan, Ming, and Qing dynasties. F (K2O, CaO, Al2O3) < 85.1 indicates that the dynasty is either Yuan or Ming. If F (K2O, CaO, Al2O3) > 85.1, the Qing dynasty can be determined (Wen et al., 2019).

$$F(K_2O, CaO, Al_2O_3) = 5.37K_2O + 4.1CaO + 2.81Al_2O_3 \quad (1)$$

The above formula (1) showed the value for porcelain sherd 2 is 79.70 and determined the dynasty of Ming from Jingdezhen, South China. Since this analysis is only valid for Chinese porcelains, it cannot be applied to sherd 1.

Aesthetic View Analysis

The morphological characteristics of ceramic bodies, such as their porosity and pore size, are determined by the topographies of the pore-formers and the removal of pore-former particles during various sintering processes. Ceramics' microstructure, porosity, and mechanical qualities can be affected by the pore-quantity, the former's chemical makeup, and temperature parameters (Obada et al., 2017). Because of the weathering conditions throughout the burial period, ancient pottery often suffers color deterioration (Xanthopoulou V et al., 2020). Techniques for surface treatment, such as smoothing and burnishing, aid in defining the social, cultural, and

economic state of an ancient culture (Corina & Volker, 2020).

Partially (sherd 2) or fully and no burnish (sherd 1) burnished surfaces are present on the outside. The predominant texture is fine, quartz-rich sand for both sherds. Many of the specimens are burnished on every surface, making it difficult to pinpoint the exact shaping method used on them. The sherd 2 must be low-fired to produce a burnish of high quality (Figure 1). Low-quality burnish is found at higher temperatures for sherd 1 (Corina & Volker, 2020). The slow-wheel technique is only evident in a small number of specimens. According to the shape of the burnished surface, both ceramic sherds are manufactured on a potter's wheel (Rangkuti & Fauzi, 2019). While partially burnished containers are ornamented with a variety of designs made up of linear scores, punctate marks, lines of punctate marks, impressed circles, and geometric-incised marks, fully burnished containers have a plain surface (Rangkuti & Fauzi, 2019). Sherd 2 has some motifs according to the design with blue and white color stoneware ceramics and no motif or design is found in sherd 1.

The majority of the vessels in this category were fired in a reducing atmosphere, but a minor number of them also show signs of having been fired in a transitional environment between reducing and oxidizing. The dark gray tone for sherd 1 as well as the smooth surface, and dense structure of the potsherds in this group make them simple to identify (Rangkuti & Fauzi, 2019). Ceramic sherd 1 shown in Figures 1 a and b is a fragment of a sizable jar or bowl (Rangkuti & Fauzi, 2019). The sherd vessel has a rough, porous external surface, and no decoration. They were made using the slow-wheel or potter's wheel and fired in an oxidizing or reducing atmosphere. This sherd's substance and shape are like burial jars from paleometallic sites in South Sumatra (Rangkuti & Fauzi, 2019). The sherd 1 reddish color was caused by the incorporation of hematite (iron oxide) by freshly created calcium and alumina silicates (Gliozzo, 2020). Most of the FPW that was excavated is "red" slipped and burnished. By Indonesian archaeologists, a different form of FPW is frequently referred to as "white" due to stylistic similarities (Ueda et al., 2017). The raw materials required to make red FPW are arguably more generally available in the area than those required to make white FPW made of nearly pure kaolin. This matches sherd 1 closely (Ueda et al., 2017). The color of the sherds can be compared in Figure 1. According to morphological analysis of ceramic earthenware for sherd 1, the fragments of the ceramic object are excavated from the coastal area of South Sumatra (Rangkuti & Fauzi, 2019) with production dates spanning the ninth to the fourteenth century CE (Husni et al., 2019).

Sherd 2 shown in Figures 1 c and d is a fragment of a bowl with a base. The blue and white porcelain pottery fragments came from plates and bowls, according to the findings of the morphological examination (Husni et al., 2019). The blue and white underglaze porcelain body contains a smooth surface with motif decoration on both the inside and outside of the sherd. On both the inside and outside of the shape, geometric themes were the most common ornamentation. On both the exterior and interior of these pieces, floral designs were the most typical ornamentation (Husni et al., 2019). For sherd 2 the ceramics were thought to have come from the Jingdezhen kiln in the early Ming Dynasty based on their quality. The ceramic vessel of sherd 2 was made on a potter's wheel and hand-painted and cobalt oxide is responsible for the blue color (Wen et al., 2019; Widjaja, G.H. Lim, Q. Lim, Mashadi, & Garland, 2011; Kock & De Waal, 2007) and potter's wheel produced ceramics that resembled finer Ming porcelains by having hand-painted, underglaze cobalt blue designs on a white background (Witkowski, 2016). At the ceramic/glaze interface of underglaze blue porcelain shards from the Ming dynasty period in China, the blue pigment is penetrated through the glaze (Kock & De Waal, 2007).

Density and Porosity Measurement

Physical characteristics like density and porosity were measured by Archimedes' Law and water absorption, respectively. The density of the ceramic sherds is 2.2 gm/cm3 and 2.3 gm/cm3 and the porosity of the ceramic sherds is 6.40% and 1.16% which indicates that ceramic sherd 1 is more porous than ceramic sherd 2. The thickness of the sherds is 5.1 mm and 5.9 mm. The vessel from which sherd 1 originated can not have been suitable to contain liquid-type materials. Bulk density, apparent porosity, and shrinkage measurements were used to evaluate the maturation characteristics of burned ceramics. Ceramic qualities like bulk density and shrinkage increase with firing temperature while apparent porosity decreases (Abubakar et al., 2020). A ceramic object's porosity is influenced by both the firing conditions and its chemical and phase composition. Since the clays expand during the dehydroxylation process, it is well understood that the porosity increases because of the high-temperature kaolinite decomposition and metakaolin production. However, the ceramics get denser and less porous when the firing temperature is further increased (Drebushchak et al., 2018).

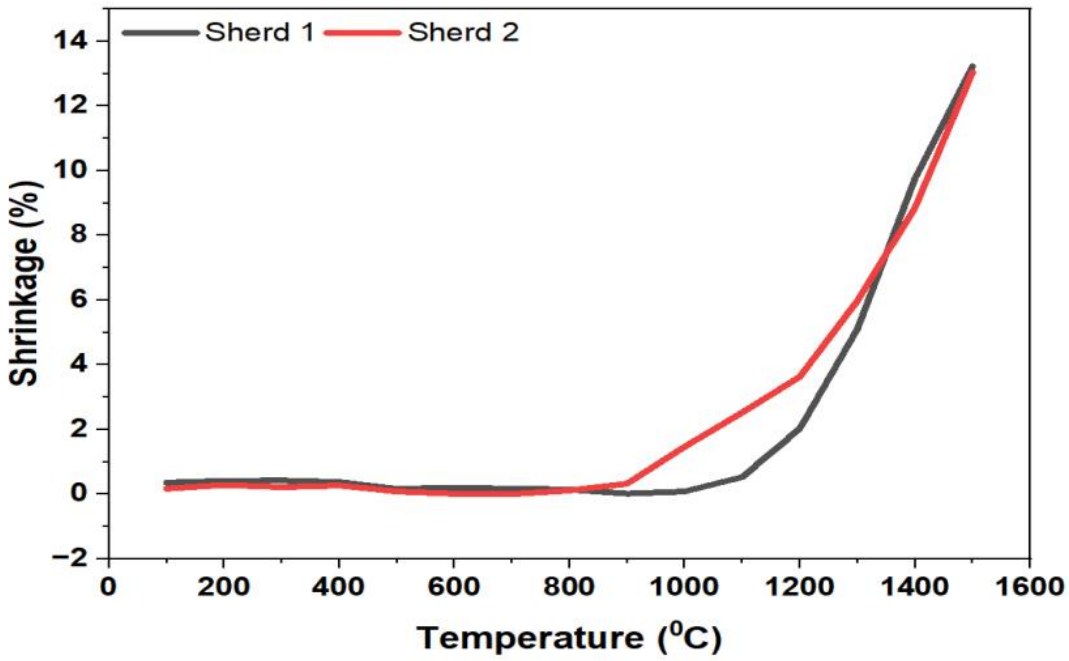

Figure 3. Temperature vs. Shrinkage of Ceramic Sherds 1 and 2 Considering Density

The shrinkage increases with temperatures in a linear function. The shrinkage is determined on samples up to 1500 °C using TMA. The density is increased, and porosity is decreased which we observe in only linear shrinkage with temperature (Drebushchak et al., 2018). Sherds 1 and 2 showed almost the same shrinkage at a temperature of 1500 °C. Sherd 1 showed an increase in density later than sherd 2 as the original firing had been at a higher temperature. Sherd 1 showed an increase in shrinkage and increase in density from temperatures 844 °C and sherd 2 showed an increase in shrinkage and increase in density from temperatures 1004 °C (Zouaoui & Bouaziz, 2017).

The behavior of porosity and density is like that of linear shrinkage, as seen in Figure 3. The linear shrinkage rises as the firing temperature rises and reaches a maximum of 1500 °C. If the heating temperature rises above 1000 °C for sherd 2. Ceramics made with kaolin are porous. As a result, there will be breakages during production, delivery, and use. Thus, it is necessary to link the mechanical characteristics of porous clay ceramics to their porosity (Obada et al., 2017). Porosity plays a significant role in the mechanical characteristics of porous ceramics, which are mostly dependent on porosity rather than simple factors like density, shrinkage, and water absorption. The presence of surface and internal flaws (such as cracks) during production and transportation are additional potential factors that could have an impact on the mechanical strength of porous ceramics (Obada et al., 2017).

Chemical Structure Analysis (FTIR)

FTIR qualitative study generated estimations based on the existence, location, and form of specific infrared absorption peaks connected to clay minerals (Yan, Liu, Chastain, Yang, & Chen, 2021). Bands overlapping in the spectrum make FTIR analysis challenging when determining the specific composition of complicated mixtures, such as archaeological ceramics. According to the FTIR pattern, presented in Figure 4, ceramic sherds 1 and 2 show the same mineralogical components in the sample which indicates quartz at peaks 434 and 439 cm-1 (Si-O bending vibrational bands (Daghmehchi et al., 2023), (Fierascu et al., 2020). Sherd 1 shows a peak of 453 cm-1 indicating the quartz with (Si-O) band (Fierascu et al., 2020) and Si-O vibrational band at a peak of 1032 cm-1 up to temperature 1200 °C (Yan et al., 2021). Both sherds contain quartz (Si-O absorption) peak at 520 cm-1 which disappears at temperatures above 500 °C (Yan et al., 2021). 672, 677, 692, and 693 cm-1 (Si-O bending), (Medeghini, Sala, De Vito, & Mignardi, 2019), 1070 and 1165 cm-1 (Bahçeli et al., 2016) show quartz. The doublet peaks of 778 and 798 cm-1, 779 and 798 cm-1 (Si-O broad) quartz has lower intensity respectively sherd 1 and sherd 2 indicating a firing temperature of more than 900 °C (Daghmehchi, Rathossi, Omrani, Emami, & Rahbar, 2018). The quartz (Si-O-Si absorption) is shown at a peak 1089 cm-1 sherd 1 at a temperature below 800 °C (Yan et al., 2021). A peak at 536 cm-1 indicates the Si-O-Al vibrational band of gehlenite at temperatures above 1200 °C (El Korhani et al., 2019). Sherd 1 shows an albite mineral (O-Si-O bending) at the peak of 579 cm-1 (Bahçeli et al., 2016), and 594 and 767 cm-1 show albite (Si-Si stretching) for sherd 2 (Bahçeli et al., 2016). Anorthite mineral found at peak 751 (Si-Al(Si) stretching) cm-1 for sherd 1 and for sherd 2 at 669 cm-1 shows anorthite with Al(Si)-O stretching band (Daghmehchi et al., 2018). Diopside (S-O-Si bending) is found at a peak of 632 cm-1 (Medeghini

et al., 2019) and peaks of 891 and 899 cm-1 indicate diopside minerals of Si-O-Si stretching band (Medeghini, Mignardi, De Vito, & Conte, 2016). A strong intensity peak of 1080 cm-1 (Si-O-Si absorption) indicates wollastonite, a calcium inosilicate, which forms at the heated temperature of over 800 °C for sherd 1 (Yan et al., 2021). The broader asymmetric-shaped Si-O band was located at a center at 1060 cm-1 because the firing temperature was high enough (T > 800 °C) to promote the sintering process and the crystallization of Ca-Al silicate minerals like diopside, gehlenite, and anorthite (Daghmehchi et al., 2018) for sherd 1. The gradual decomposition of quartz from 800 to 1100 °C, which evidence was caused by the quartz reaction with gehlenite to generate wollastonite and anorthite, was followed by a significant reduction at 1100 °C (Gliozzo, 2020). The peaks 1083 and 1176 cm-1 show the quartz with Si-O asymmetric stretching band at temperatures 700 °C - 750 °C (Daghmehchi et al., 2018). The peak at 553 cm-1 for sherd 1 and 558, 460 cm-1 for sherd 2 identified the hematite (Fe-O stretching) (Fierascu et al., 2020) due to the chemical composition of Fe2O3 in sherds as found by XRF. Table 3 represents the wavenumbers with mineralogical vibrational assignment of ceramic sherds.

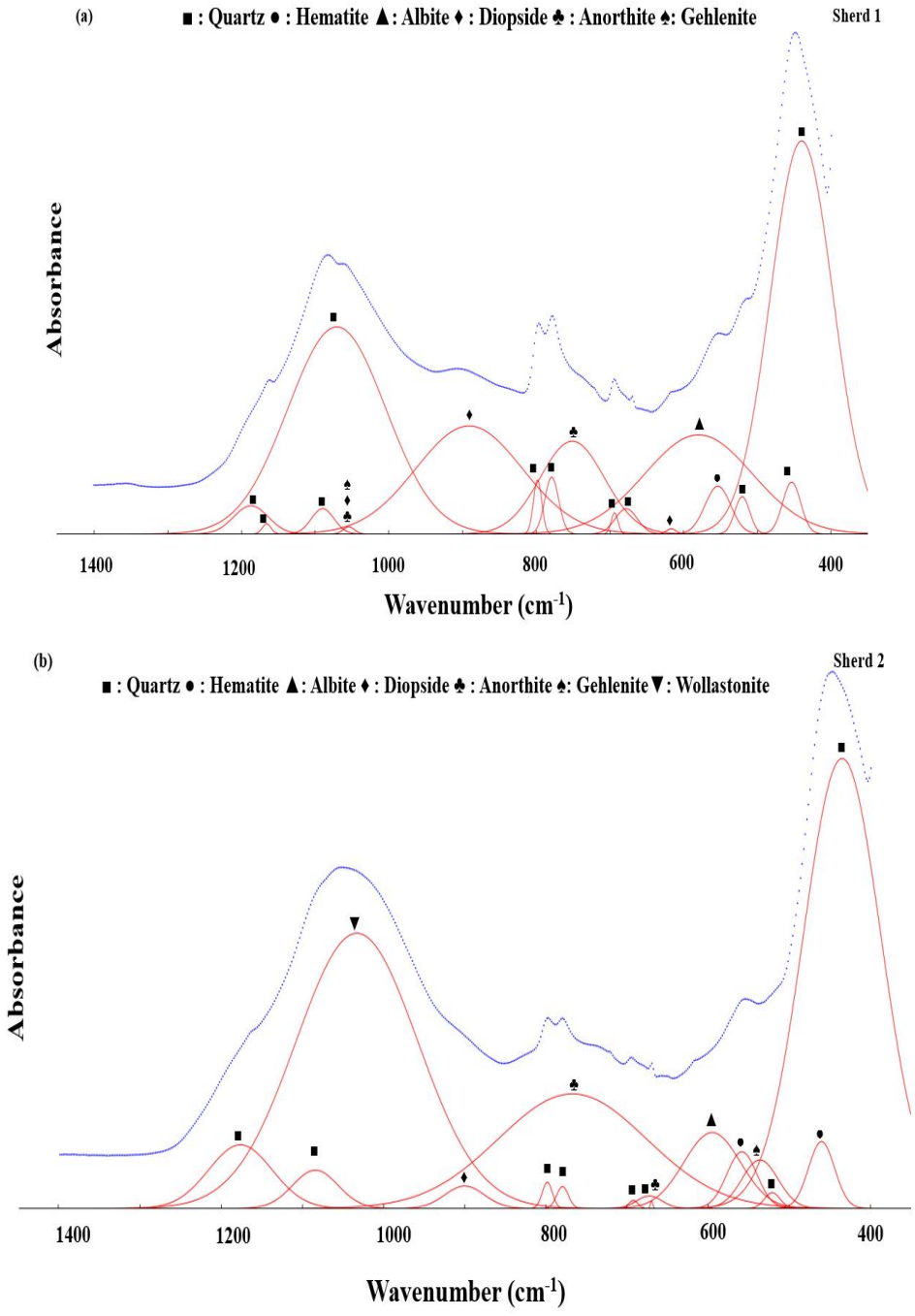

Figure 4. FTIR Spectrum of (a) Sherd 1 And (b) Sherd 2

Table 3. FTIR Wavenumbers (cm-1) of Sherds with Corresponding Vibrational Assignments and Minerals

FTIR absorption bands in wavenumbers (cm^{-1}) with a comparative intensity		Vibrational assignment	Mineral	References
Sherd 1	Sherd 2			
1176 W	1176 W	Si-O absorption	Quartz	(Bahçeli et al., 2016; Ricci et al., 2016)
	1080 M	Si-O-Si absorption	Wollastonite	(Yan et al., 2021; Fierascu et al., 2020)
1060 VS		Si-O broadband	Diopside	(Dey, Coleman Carter, and Swift, 2020; Daghmehchi et al., 2018)
	1036 VS	Si-O-Si stretching	Kaolinite	(Lettieri and Giannotta, 2017; Ricci et al., 2016; El Korhani et al., 2019; Bahçeli et al., 2016; Yan et al., 2021)
881 W	885 W	Si–O–Si stretching	Diopside	(Medeghini et al., 2016)
798 W	798 M	Si–O–Si stretching	Quartz	(Bahçeli et al., 2016; Ricci et al., 2016; Lettieri and Giannotta, 2017; Medeghini et al., 2016; Fierascu et al., 2020; Dey, Coleman Carter, and Swift, 2020; Daghmehchi et al., 2018; Fatima Elbashir Siddig, 2019; Fabbri, Gualtieri, and Shoval, 2014; Kazakou et al., 2019; R. Palanivel and U. Rajesh Kumar, 2011)
777 W	779 M	Si–O–Si stretching	Quartz	(Bahçeli et al., 2016; Ricci et al., 2016; Lettieri and Giannotta, 2017; Medeghini et al., 2016; Fierascu et al., 2020; Dey, Coleman Carter, and Swift, 2020; Daghmehchi et al., 2018; Fatima Elbashir Siddig, 2019; Fabbri, Gualtieri, and Shoval, 2014; Kazakou et al., 2019; R. Palanivel and U. Rajesh Kumar, 2011)
764 M	764 M	Si-Si stretching	Albite	(Bahçeli et al., 2016; Medeghini et al., 2016)
692 VW	694 VW	Si-O bending	Quartz	(Bahçeli et al., 2016; Ricci et al., 2016; Fatima Elbashir Siddig, 2019; Kazakou et al., 2019)
677 W	672 W	Si-O bending	Quartz	(Medeghini et al., 2019; Bahçeli et al., 2016)
	667 VW	Al(Si)–O stretching	Anorthite	(Medeghini et al., 2016)
579 M	585 W	O-Si-O bending	Albite	(Bahçeli et al., 2016)
559 M	558 M	Fe-O stretching	Hematite	(Dey, Coleman Carter, and Swift, 2020; Bahçeli et al., 2016; Yan et al., 2021)
	533 VW	Si-O-Al bending	Gehlenite	(Medeghini et al. 2019)
520 W	520 W	Si-O bending	Quartz	(Bahçeli et al., 2016; Fierascu et al., 2020; El Korhani et al., 2019)
	460 W	Fe-O stretching	Hematite	(Fierascu et al., 2020; Bahçeli et al., 2016)
434 S, 450 S	439 S	Si-O bending	Quartz	(Fierascu et al., 2020; El Korhani et al., 2019; Kazakou et al., 2019).

*S: Strong, VS: Very Strong, M: Medium, W: Weak, VW: Very Weak

Mineralogical Phase Analysis (XRD)

The samples consist of quartz, clay minerals, and feldspar shown in the XRD pattern. The dominant phase of the sample is quartz shown in FTIR as well as XRD. Based on their preferred orientation, selected diffractograms of ceramic samples show all major crystalline phases (Maged, Abu El-Magd, Radwan, Kharbish, & Zamzam, 2023; Omar, 2022). Two groups of phases are seen in terms of the thermodynamics of mineral occurrences. The first group consists of low-temperature phases that were utilized as fillers or minerals connected to the raw materials (such as quartz, calcite, and muscovite). The second category consists of high-temperature phases formed by partial sintering and recrystallization, such as diopside, gehlenite, and hematite (Emami, Sakali, Pritzel, & Trettin, 2016).

The close spacing between reflections in the diffractogram caused quartz and mullite to overlap each other primarily as well as diopside and gehlenite (Emami et al., 2016). A low intensity of hematite indicates after the

iron in the clay's crystal structure was leached out by weathering caused by exposure to moisture or acidic drainage (Emami et al., 2016).

The only phases from the raw material left are quartz, albite, and muscovite with distinct crystal planes, whereas the other phases are produced during firing. Diopside was the new crystalline phase rebuilt within the structure as detected through X-ray diffraction. The final stages of high-temperature fresh recrystallization in the ceramic texture diopside (Emami et al., 2016) from reddish yellow to very pale brown due to the crystallization of diopside and gehlenite in an oxidizing atmosphere as mentioned above (Daghmehchi et al., 2018). Gehlenite is a sorosilicate with the chemical formula Ca2Al(AlSiO7) that is formed when clay and calcium carbonate combine at a temperature of 750 °C to 850 °C (Pradell & Molera, 2020). Both ceramic sherds showed gehlenite phases in the XRD pattern because natural clay is used in ancient ceramics (Pradell & Molera, 2020). High-temperature fire is associated with the formation of gehlenite, which results from the reaction of SiO2, Al2O3, and free CaO with clay and carbonate minerals (Botticelli et al., 2020). Since generated phases like anorthite normally form above 850 °C, sherd sample 2 lacked them, which shows that the firing temperature of 850 °C was not exceeded (Botticelli et al., 2020). Sherds 1 associated anorthite in the XRD pattern which indicated higher sintering temperature explained by the TMA curve in Figure 5.

The bodies of the Jingdezhen underglaze blue porcelains were made from porcelain stone (Tite et al., 2012). Quartz is abundant, with high SiO2/Al2O3 weight percent concentration and high ratios (around 5:1) surrounding the quartz particles. Generally, quartz is more prevalent in porcelain, and feldspar crystal shards are less common in underglaze blue porcelain. Quartz's highest point has an intensity that indicates that of the Jingdezhen-produced Qing dynasty porcelain (Prinsloo et al., 2005). The lower percentage of mullite which comes from alumina (Al2O3) in sherd 2 originated from Southern China of porcelain ceramics. Similar XRD patterns for these ceramics reveal the presence of gehlenite (Ca2Al2SiO7), and diopside (CaMgSi2O6) (Figure 5). The quartz shows the highest pattern in both ceramics' patterns with different intensity peaks, sherd 1 is very sharp than 2 with Quartz peak intensity having a high tendency to decline. The phase composition of sherds shown in Table 4.

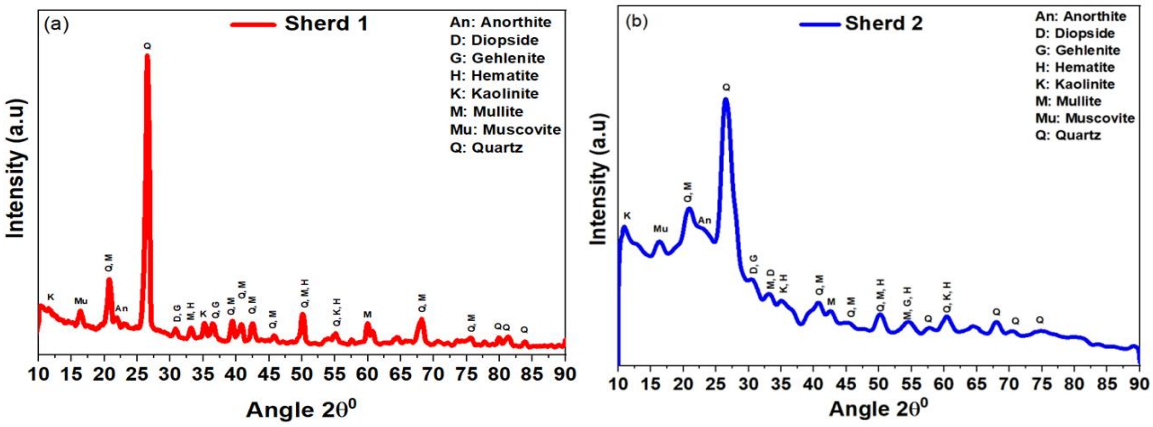

Figure 5. XRD Analysis of (a) Sherd 1 and (b) Sherd 2

Table 4. Phase Composition of Ceramic Sherds

Minerals	Chemical Formula	Phase Quantity (wt.%)		Code Number	Code Reference
		Sherd 1	Sherd 2		
Anatase	TiO2	0.21	0.53	7206075	(Rezaee et al., 2011)
Anorthite	CaAl2Si2O8	2.03	12.90	9005309	(Matsui & Kimata, 1997)
Diopside	MgCaSi2O6	1.67	1.47	1000007	(Thompson & Downs, 2008)
Gehlenite	Ca2Al[AlSiO7]	0.68	00	1000048	(Swainson et al., 1992)
Kaolinite	Al2Si2O5(OH)4	2.83	3.83	1550598	(Richard & Rendtorff, 2019)
Mullite	3Al2O3 2SiO2	32.60	35.30	7105575	(Zhang et al., 2010)
Muscovite	Al3H2KO12Si3	9.40	4.38	9015970	(Mesto et al., 2012)
Quartz	SiO2	50.62	41.56	9013321	(Antao et al., 2008)

Thermal Analysis (TMA)

The TMA process is time-dependent on applying a very small force to investigate sintering temperature, phase changes, cracking, and quartz inversion (Štubna, Trník, & Vozár, 2009). Ceramic technological studies have focused heavily on estimating the firing temperature utilized in the production of pottery and the association between the firing environment and color (Tite, 2008). According to Figure 6 (a), sherd 1 showed the sintering starting temperature at 1000 °C with high temperature which indicates the earthenware (Emami et al., 2016).

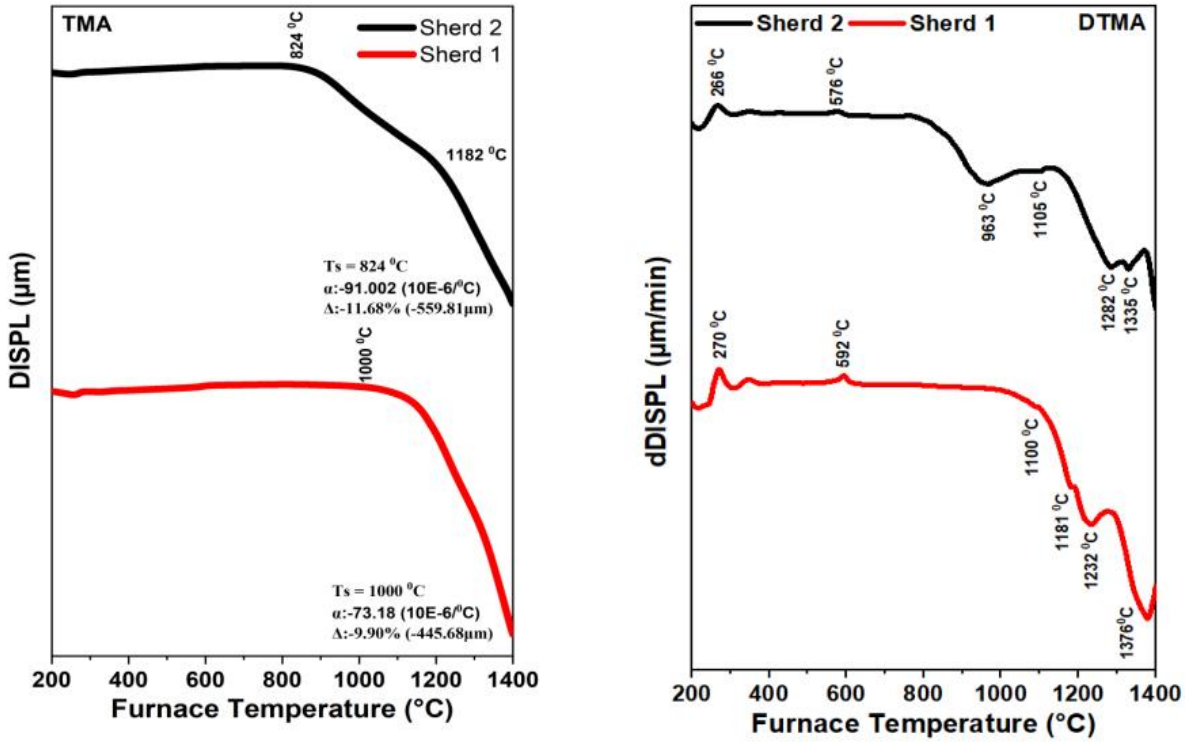

Figure 6. Thermal Analysis Curve of Sherds (a) TMA (b) DTMA.

According to Figure 6, ceramic sherd 1 showed sudden expansion from 179 °C up to 183 °C. The transition temperature starts from 183 °C and up to 1000 °C. The deformation point is 1000 °C. Softening point at 1000 0C. The shrinkage percentage at the slope area of changes is (29%) and the total shrinkage is (10%). The coefficient of thermal expansion is (73 x 10-6 °C-1).

Similarly, sherd 2 showed a sudden expansion from 173 °C up to 181 °C. The transition temperature starts from 181 °C and up to 814 °C. The deformation point is 824 °C. Shrinkage starts at 824 °C up to 1499 °C, shrinkage percentage at the last point is (13%). At shrinkage area at one point breaks the profile at 1182 °C. Softening point at 824 °C. The shrinkage percentage at the slope area of changes is (13%) and the total shrinkage is (12%). The coefficient of thermal expansion is (91 x 10-6 °C-1).

The many techniques used in antiquity to establish the firing temperatures all require finding a correlation between the firing temperature and changes in the pottery's mineralogy or microstructure. The pottery's clay matrix undergoes gradual sintering and vitrification, which are considered microstructural changes (Tite, 2008). According to the TMA curve, the ancient ceramic artifacts required high temperature which indicates a higher temperature kiln is required for the artifacts. The DTMA curve shows the peaks at temperatures of sherd 1 and 2 at peaks at 576 °C and 592 °C for the inversion of quartz and the mullite crystallization happened around 1200 °C (Húlan, Štubňa, Al-Shantir, & Trník, 2023; Gliozzo, 2020; Ion et al., 2011; Drebushchak et al., 2018; Mammadov & Ahadova, 2023). According to TMA curves, the mullite crystallization happened around 1200 °C (Albuquerque et al., 2004). Quartz content rose from 800 to 900 °C and fell from 900 to 1100 °C. The tendency to decrease at high temperatures is brought on by the development of silica melt because of the alkaline feldspars' function as fluxing agents (producing mullite) (Gliozzo, 2020). The polymorphic change of mullite from its cubic to orthorhombic form can account for the peak maximum at 1250 °C in DTMA (Chakraborty, 1992). A Little peak of 266 °C and identify a small amount of water elimination which indicates the pure porcelain of ceramic (Wu et al.,

2015) sherd 2 whereas sherd 1 has a relatively higher peak. The exothermic peak from 1150 °C-1400 °C exhibits the transformation from kaolinite to mullite production (Chakraborty, 1992). Mullite is an acicular crystal that is very visible and desired after thermal heat treatment because of its thermal and mechanical qualities (Harrati, Manni, El Bouari, El Hassani, & Sadik, 2019). The XRD pattern shows a higher percentage of mullite in sherds. The fired clay over 800 °C produces new minerals such as gehlenite, anorthite, diopside, and wollastonite (Fabbri et al., 2014). These minerals were found in XRD patterns and FTIR spectra.

The ceramic artifacts have a high iron content and are low in calcium. The method of firing can be determined by the presence of hematite in all samples. most probable, the process ended in an oxidizing environment. It must also be mentioned, that in Ca-poor ceramics, the hematite content was found to rise with the firing temperature (Lahlil, Bouquillon, Morin, Galoisy, & Lorre, 2009). The sherd 1 a with a high iron oxide indicates a higher percentage of hematite in the XRD pattern and the amount of Fe_2O_3 is higher and CaO with a lower percentage by XRF.

Summary of Characterization Analysis

In summary, after vitrification, the porosity dramatically decreases. Due to their fluxing action, alkaline-rich phases (K_2O) in the fired sample cause the vitrification process to accelerate (Zouaoui & Bouaziz, 2017). The higher amount of K_2O in sherd 2 (4.57%) than in sherd 1 (1.78%) indicates more porosity found at sherd 1 as well as a lower required sintering temperature in sherd 2. Vitreous phase development might also result from the release of amorphous silica during the breakdown of metakaolin. The processes that occur in porcelain mixture during its firing up to 1000 °C can be represented by a curve. These processes include the release of physically bound water at temperatures between 20 and 150 °C, dehydroxylation at temperatures above 400 °C, collapse of a meta kaolinite lattice at 950 °C, and the formation of spinel and mullite (Štubňa et al., 2009). Once crystalline kaolin, metakaolin has since undergone an amorphous transformation. This explains the less intense kaolin peaks that are seen in the X-ray patterns of ceramics as well as why some of the peaks that are easily visible in kaolin are not noticeable. After thermal treatments, the phases of the porous ceramic samples indicate the transition phase to mullite (Obada et al., 2017) which should happen at or around the temperature utilized in this study for sherd 1 and sherd 2 are 1095 °C and 1122 °C.

Iron oxides in the raw materials (5.53%, Fe_2O_3), in the form of hematite, caused the hue to be primarily red in sherd 1 of earthenware. The difference in color can also be attributed to the presence of more oxide impurities, such as titanium (TiO_2) minerals, magnesium (MgO), aluminium oxide (Al_2O_3), or temperature, but most notably to calcium (2.43%, CaO), whose presence in significant amounts lessens the effect of iron on the production of red or pink color for sherd 2 porcelain (Kagonbé, Tsozué, Nzeukou, & Ngos, 2021). Cobalt blue and copper red decorations were created on stoneware and porcelain in China during the Ming dynasty, with a variety of outcomes. The interaction of the cobalt pigment with the body of the porcelain is observed to produce blue color which was identified (Pradell & Molera, 2020) at sherd 2. The reddish-brown clay used to create the pottery is shared by them with earlier Chinese cultures, and they initially resemble ceramics from Western Asia and the Mediterranean (Liritzis & Westra, 2022). The early research mostly concentrated on the application of cobalt to the colouring of pottery in Mediterranean archaeological sites. Since only Persian cobalt sources have been thoroughly researched, our comments will mostly address the Asian region (that is, Turkey, Iran, China, Vietnam, and Japan) and its interactions with other regions, especially with Europe (Colomban et al., 2021).

The primary components of raw clay materials such as clay minerals, quartz, feldspar, and calcite become less stable during the firing process. They partially decompose and interact with one another to create new mineral phases such as mullite, and wollastonite under high-temperature conditions (El Idrissi et al., 2018). The mineral's transformation from one stage to another phase is clearly described in the TMA process with temperatures at higher than 1000 °C As well as shown in the XRD pattern. The wollastonite is found in earthenware sherd 1 at high temperatures displayed in the FTIR pattern. The existence of freshly produced phases, particularly wollastonite, is thoroughly established at 1100 °C. The technological features of materials that define their application in the creation of earthenware products are largely influenced by their chemical and mineralogical composition (El Idrissi et al., 2018) for sherd 1.

A lower percentage of CaO less than 5% of both sherds are non-calcareous refractory clays used for ceramic production (Tite, 2008). Southern China created porcelains in Jingdezhen using porcelain stone, which is made up of a fine aggregate of quartz, muscovite (potash mica), albite (sodium feldspar), and, occasionally, kaolinite (Tite, 2008). The porcelain sherd indicates the origin of South China because of the abundant amount shown in XRF and the high intensity of quartz in the XRD pattern. Albite mineral is shown in broad peaks for sherd 2 in the FTIR pattern. The investigation of the cobalt blue pigment used for the underglaze decoration in the blue-and-white Ming dynasty of China was another early study of Chinese porcelain.

Quartz inclusions lessen the flexibility of clay, which has the effect of preventing shrinkage and cracking after burning. Because of this, they have been used frequently throughout history. Inclusions of $CaCO_3$ were utilized to make ceramics in antiquity at low temperatures when $CaCO_3$ breaks down to CaO, which acts as a flux and induces low-temperature sintering. The high percentage of CaO acts as a flux for sherd and works at low temperatures (Kazakou et al., 2019). Gehlenite loses stability at 1000 °C and its modal amount significantly drops. This is probably related to the onset of anorthite and wollastonite formation, which is demonstrated in ceramic sherd 1 of earthenware ceramic, whose reflect intensities increase at 1050 °C (Daghmehchi et al., 2018). Gehlenite and calcite are signs that the pieces were fired at temperatures between 850 °C and 900 °C. The presence of diopside indicates that ceramics could not have been fired below 800 °C (Lahlil et al., 2009). The ancient ceramic items are fragile and porous. They were made from calcareous clay that had a high iron content and was fired in an oxidizing atmosphere at relatively low temperatures, between 700 and 850 °C. The original ceramic paste contained substantial amounts of quartz and calcite inclusions. The earthenware type of ceramics used nowadays is less porous, more durable, and less brittle. They were produced by firing earthen clay in an oxidizing atmosphere at temperatures exceeding 1000 °C (Kazakou et al., 2019). In comparison to present efforts, the proposed methodology contributes most significantly to the characterization of ceramics by helping to determine the firing temperature of raw materials through the analysis of the mineral assemblages (Liritzis et al., 2020).

The study of ceramics is applied by the curator, archaeologist, scientist, and geologist to identify the ceramic artifacts dating using various traditional techniques and approaches. Considering various experienced data and information, several processes are applied to identify ceramic artifacts' origin, dating, and characteristics. The maximum ceramic is identified by professional archaeologists mostly by significant visual identification. Visual identification is closely related to the aesthetic view, colors, manufacturing system, size, texture, and uses of ceramic artifacts (Corina & Volker, 2020; Dias et al., 2013). The Traditional identification method exhibits sometimes less reliability and inconsistent accuracy in the ceramic dating process. When scientific methods are used on ancient pottery, it is hoped that this would increase their worth by revealing details about their history, technology, and underlying cultural significance. A combination of aesthetic art history and scientific characterization techniques of ceramic artifact analysis approaches reflect a novelty in the study. These results showed that two ancient ceramic sherds were characterized based on FTIR, XRD, and TMA techniques. The different mineralogical and phase changes in ceramic sherds provide an essential catheterization related to the temperature of sintering and deformation temperature in an ancient kiln. A higher temperature was required for sherds with a change of phase such as diopside, gehlenite, and anorthite. Most of the ancient ceramics required higher temperatures in firing manufacturing procedures. This study was analyzed based on ceramic porcelain and earthenware of ceramic sherds as well as the typology of expert opinions for provenance, dating, and characterization. In the future, a combination of different scientific analytical approaches may provide a much more and clearer synergy of characterization for reducing the ambiguities of different sherd analytical approaches in material science.

CONCLUSION

In this study, the mineralogical and thermal analysis of ceramic artifacts were analyzed. The gehlenite, diopside, and mullite showed at higher temperatures while the quartz and kaolinite transformed at lower temperatures. For both ceramic sherds, silicon is abundant in more than 70% of the total clay. The thermal behaviors of ancient ceramics were different as well as different kilns were used during firing. Both analyses approaches, generally provided the ceramics' origin, age, and sintering temperature which depends on the internal phase change of minerals and manufacturing techniques as well as an aesthetic view of different regimes. However, morphological, and aesthetic analysis of the sherd for color effect which scientifically developed by examining the chemical composition of ceramic materials. Cobalt blue for blue-white porcelain and a high amount of iron oxide for reddish color. Also, the addition of the FTIR and XRD spectra determined the minerals associated with temperature and chemical bond structure. The earthenware ceramics were produced at a higher temperature while the blue-white porcelain was produced at lower temperatures than earthenware with kaolinite clay. Increasing the temperature gradually increased the ceramic contraction for both ceramics. The earthenware ceramic is more porous and has a lower density than porcelain. Therefore, they showed archaeological evidence with a scientific application where a combination of traditional and modern approaches is desired.

AUTHOR CONTRIBUTIONS

Conceptualization, H.S.C.M.; methodology, H.S.C.M. and M.S.R.; software, H.S.C.M. and M.S.R.; validation, M.S.R., H.S.C.M. and B.B.A.R.; formal analysis, M.S.R.; data curation, H.S.C.M.; writing—original draft preparation, M.S.R.; writing—review and editing, M.S.R., H.S.C.M. and B.B.A.R.; visualization, H.S.C.M.; supervision, H.S.C.M.; project administration, H.S.C.M. All authors have read and agreed to the published version of the manuscript.

ACKNOWLEDGEMENTS

This study is fully funded by the Impact-Oriented Interdisciplinary Research Grant Programme (IIRG), Universiti Malaya Grant Number IIRG008C-19SAH and partially supported by IIRG034B-2019.

CONFLICT OF INTEREST

The authors declare that they have no known competing financial interests or personal relationships that could have appeared to influence the work reported in this paper.

REFERENCES

Abubakar, M., Muthuraja, A., Rajak, D. K., Ahmad, N., Pruncu, C. I., Lamberti, L., & Kumar, A. (2020). Influence of firing temperature on the physical, thermal and microstructural properties of kankara kaolin clay: A preliminary investigation. *Materials*, *13*(8), 1872.

Albuquerque, F., Parente, B., Lima, S., Paskocimas, C., Longo, E., Souza, A., . . . Fernandes, V. (2004). Thermal transformations of tile clay before and after kaolin addition. *Journal of Thermal Analysis and Calorimetry*, *75*(2), 677-685.

Antao, S. M., Hassan, I., Wang, J., Lee, P. L., & Toby, B. H. (2008). State-of-the-art high-resolution powder X-ray diffraction (HRPXRD) illustrated with rietveld structure refinement of quartz, sodalite, tremolite, and meionite. *The Canadian Mineralogist*, *46*(6), 1501-1509.

Bahçeli, S., Güleç, G., Erdoğan, H., & Söğüt, B. (2016). Micro-Raman and FT-IR spectroscopic studies of ceramic shards excavated from ancient Stratonikeia city at Eskihisar village in West–South Turkey. *Journal of Molecular Structure*, *1106*, 316-321.

Baziotis, I., Xydous, S., Manimanaki, S., & Liritzis, I. (2020). An integrated method for ceramic characterization: A case study from the newly excavated Kastrouli site (Late Helladic). *Journal of Cultural Heritage*, *42*, 274-279.

Botticelli, M., Mignardi, S., De Vito, C., Liao, Y., Montanari, D., Shakarna, M., . . . Medeghini, L. (2020). Variability in pottery production at Khalet al-Jam'a necropolis, Bethlehem (West Bank): From the early-middle bronze to the iron age. *Ceramics International*, *46*(10), 16405-16415.

Chakraborty, A. K. (1992). Resolution of thermal peaks of kaolinite in thermomechanical analysis and differential thermal analysis studies. *Journal of the American Ceramic Society*, *75*(7), 2013-2016.

Chenoweth, J. M., & Farahani, A. (2015). Color in historical ceramic typologies: A test case in statistical analysis of replicable measurements. *Journal of Archaeological Science: Reports*, *4*, 310-319.

Chew, S. C. (2018). The Southeast Asian connection in the first Eurasian world economy 200 BC AD 500. *Comparing Globalizations: Historical and World-Systems Approaches*, 91-117.

Colomban, P., Kırmızı, B., & Simsek Franci, G. (2021). Cobalt and associated impurities in blue (and green) glass, glaze and enamel: Relationships between raw materials, processing, composition, phases and international trade. *Minerals*, *11*(6), 633.

Corina, I., & Volker, H. (2020). Ceramic technology. How to investigate surface finishing. *Archaeological and Anthropological Sciences*, *12*(9).

Csáki, Š., Lukáč, F., Húlan, T., Veverka, J., & Knapek, M. (2021). Preparation of anorthite ceramics using SPS. *Journal of the European Ceramic Society*, *41*(8), 4618-4624.

Daghmehchi, M., Coletti, C., Moon, D. H., Jelodar, M. E. E., Omrani, H., Reka, A. A., . . . Emami, M. (2023). Mineralogical and microstructural characterization of ceramics from the fifth and fourth millennium BC in the central plateau of Iran. *Open Ceramics*, *15*, 100427.

Daghmehchi, M., Rathossi, C., Omrani, H., Emami, M., & Rahbar, M. (2018). Mineralogical and thermal analyses of the Hellenistic ceramics from Laodicea Temple, Iran. *Applied Clay Science*, *162*, 146-154.

Dey, T., Carter, J. C., & Swift, K. (2020). SEM-EDX and FTIR analysis of archaeological ceramic potteries from southern Italy. *Microscopy*, *69*(6), 371-380.

Dias, M. I., Prudêncio, M. I., De Matos, M. P., & Rodrigues, A. L. (2013). Tracing the origin of blue and white Chinese Porcelain ordered for the Portuguese market during the Ming dynasty using INAA. *Journal of Archaeological Science*, *40*(7), 3046-3057.

Doebelin, N., & Kleeberg, R. (2015). Profex: A graphical user interface for the rietveld refinement program BGMN. *Journal of Applied Crystallography*, *48*(5), 1573-1580.

Drebushchak, V. A., Mylnikova, L. N., & Drebushchak, T. N. (2018). Thermoanalytical investigations of ancient ceramics: Review on theory and practice. *Journal of Thermal Analysis and Calorimetry*, *133*, 135-176.

El Idrissi, H. E. B., Daoudi, L., El Ouahabi, M., Collin, F., & Fagel, N. (2018). The influence of clay composition and lithology on the industrial potential of earthenware. *Construction and Building Materials*, *172*, 650-659.

El Korhani, O., Souaidan, M., Zaouk, D., Khoury, R., & Cornu, D. (2019). Characterization of natural Lebanese clays for the preparation of ceramic membranes designed to water filtration. *Lebanese Scientific Journal*, *20*, 451-467.

El Ouahabi, M., El Idrissi, H. E. B., Daoudi, L., El Halim, M., & Fagel, N. (2019). Moroccan clay deposits: Physico-chemical properties in view of provenance studies on ancient ceramics. *Applied Clay Science*, *172*, 65-74.

Elbashir Siddig, F., Elbashir, A. A., & Lepper, V. (2019). Multi-analytical approach for characterization of archaeological Meroitic potsherds. *International Journal of Experimental Spectroscopic Techniques*, *4*(1), 1-17.

Emami, M., Sakali, Y., Pritzel, C., & Trettin, R. (2016). Deep inside the ceramic texture: A microscopic–chemical approach to the phase transition via partial-sintering processes in ancient ceramic matrices. *Journal of Microscopy and Ultrastructure*, *4*(1), 11-19.

Enyuan, W., Yinfei, X., Yibing, Z., & Jingwei, W. (2021). Provenance study of ceramic sherds excavated from Qinglong Town site during Tang and Song Dynasties by composition and petrography analysis. *Journal of Archaeological Science: Reports*, *38*, 103112.

Fabbri, B., Gualtieri, S., & Shoval, S. (2014). The presence of calcite in archeological ceramics. *Journal of the European Ceramic Society*, *34*(7), 1899-1911.

Fierascu, R. C., Fierascu, I., Baroi, A. M., Brazdis, R. I., Fistos, T., Nicolae, C. A., . . . Sava, V. (2020). Characterization of historical ceramics: a case study. *Romanian Reports in Physics*, *72*(1), 801.

Gliozzo, E. (2020). Ceramic technology. How to reconstruct the firing process. *Archaeological and Anthropological Sciences*, *12*(11), 260.

Gutiérrez, A., Gerrard, C., Zhang, R., & Guangyao, W. (2021). The earliest Chinese ceramics in Europe?. *Antiquity*, *95*(383), 1213-1230.

Harrati, A., Manni, A., El Bouari, A., El Hassani, I. E. E. A., & Sadik, C. (2020). Elaboration and thermomechanical characterization of ceramic-based on Moroccan geomaterials: Application in construction. *Materials Today: Proceedings*, *30*, 876-882.

Heimann, R. B., & Maggetti, M. (2019). The struggle between thermodynamics and kinetics: Phase evolution of ancient and historical ceramics. *EMU Notes in Mineralogy, 20*(6), 233-281.

Húlan, T., Štubňa, I., Al-Shantir, O., & Trník, A. (2023). The apparatus for thermomechanical analysis of clay-based ceramics. *Measurement Science Review*, *23*(3), 130-135.

Husni, A., Ibrahim, H., & Saidin, M. (2019). An investigation of archaeological remains at Lamreh site, Aceh, Indonesia and their context within the Lamuri Kingdom. *IJAPS*, *15*(2), 59-88.

Ion, R. M., Dumitriu, I., Fierascu, R. C., Ion, M. L., Pop, S. F., Radovici, C., . . . Niculescu, V. I. R. (2011). Thermal and mineralogical investigations of historical ceramic: A case study. *Journal of Thermal Analysis and Calorimetry*, *104*(2), 487-493.

Javanshah, Z. (2018). Chemical and mineralogical analysis for provenancing of the Bronze Age pottery from Shahr-i-Sokhta, South Eastern Iran. *Scientific Culture*, *4*(1), 83-92.

Jutimoosik, J., Sirisathitkul, C., Limmun, W., Yimnirun, R., & Noonsuk, W. (2017). Synchrotron XANES and ED‐XRF analyses of fine‐paste ware from 13th to 14th century maritime Southeast Asia. *X‐Ray Spectrometry*, *46*(6), 492-496.

Kagonbé, B. P., Tsozué, D., Nzeukou, A. N., & Ngos, S. I. I. I. I. I. I. (2021). Mineralogical, physico-chemical and ceramic properties of clay materials from Sekandé and Gashiga (North, Cameroon) and their suitability in earthenware production. *Heliyon*, *7*(7).

Kazakou, T., Zorba, T., Vourlias, G., Pavlidou, E., & Chrissafis, K. (2019). Combined studies for the determination of the composition and the firing temperature of ancient and contemporary ceramic artefacts. *Thermochimica Acta*, *682*, 178412.

Kock, L. D., & De Waal, D. (2007). Raman studies of the underglaze blue pigment on ceramic artefacts of the Ming dynasty and of unknown origins. *Journal of Raman Spectroscopy: An International Journal for Original Work in all Aspects of Raman Spectroscopy, Including Higher Order Processes, and also Brillouin and Rayleigh Scattering*, *38*(11), 1480-1487.

Lahlil, S., Bouquillon, A., Morin, G., Galoisy, L., & Lorre, C. (2009). Relationship between the coloration and the firing technology used to produce Susa Glazed ceramics of the end of the Neolithic Period. *Archaeometry*, *51*(5), 774-790.

Lara, M. (2020). Ceramic abandonment. How to recognise post-depositional transformations. *Archaeological and Anthropological Sciences*, *12*(8).

Lettieri, M., & Giannotta, M. T. (2017). Investigations by FT-IR spectroscopy on residues in pottery cosmetic vases

from archaeological sites in the mediterranean basin. *International Journal of Experimental Spectroscopic Techniques*, *2*.

Lim, T. S. (2018). Chinese ceramics in Southeast Asia. In C. Smith (Ed.*), Encyclopedia of Global Archaeology* (pp. 1-12). Switzerland: Springer.

Liritzis, I., & Westra, A. J. (2022). The lower Yangtze River and Aegean Sea in the third millennium BC: Parallel cradles of civilizations. *Asian Archaeology*, *6*(1), 111-124.

Liritzis, I., Laskaris, N., Vafiadou, A., Karapanagiotis, I., Volonakis, P., Papageorgopoulou, C., & Bratitsi, M. (2020). Archaeometry: An overview. *Scientific Culture*, *6*(1).

Liritzis, I., Xanthopoulou, V., Palamara, E., Papageorgiou, I., Iliopoulos, I., Zacharias, N., . . . Karydas, A. G. (2020). Characterization and provenance of ceramic artifacts and local clays from Late Mycenaean Kastrouli (Greece) by means of p-XRF screening and statistical analysis. *Journal of Cultural Heritage*, *46*, 61-81.

Maged, A., Abu El-Magd, S. A., Radwan, A. E., Kharbish, S., & Zamzam, S. (2023). Evaluation insight into Abu Zenima clay deposits as a prospective raw material source for ceramics industry: Remote sensing and characterization. *Scientific Reports*, *13*(1), 58.

Mammadov, S., & Ahadova, A. (2023). Comprehensive investigation of Neolithic ceramic samples: Firing technology and age insights. *East European Journal of Physics*, (3), 531-534.

Matsui, T., & Kimata, M. (1997). Crystal chemistry of synthetic Mn-bearing anorthite: Incorporation of MnAl~ 2Si~ 2O~ 8 end-member into feldspar. *European Journal of Mineralogy-Ohne Beihefte*, *9*(2), 333-344.

Medeghini, L., Mignardi, S., De Vito, C., & Conte, A. M. (2016). Evaluation of a FTIR data pretreatment method for Principal Component Analysis applied to archaeological ceramics. *Microchemical Journal*, *125*, 224-229.

Medeghini, L., Sala, M., De Vito, C., & Mignardi, S. (2019). A forgotten centre of ceramic production in Southern Levant: Preliminary analytical study of the Early Bronze Age pottery from Tell el-Far ‘ah North (West Bank). *Ceramics International*, *45*(9), 11457-11467.

Mesto, E., Scordari, F., Lacalamita, M., & Schingaro, E. (2012). Tobelite and NH4+-rich muscovite single crystals from Ordovician Armorican sandstones (Brittany, France): Structure and crystal chemistry. *American Mineralogist*, *97*(8-9), 1460-1468.

Mu, T., Wang, F., Wang, X., & Luo, H. (2019). Research on ancient ceramic identification by artificial intelligence. *Ceramics International*, *45*(14), 18140-18146.

Obada, D. O., Dodoo-Arhin, D., Dauda, M., Anafi, F. O., Ahmed, A. S., & Ajayi, O. A. (2017). The impact of kaolin dehydroxylation on the porosity and mechanical integrity of kaolin based ceramics using different pore formers. *Results in Physics*, *7*, 2718-2727.

Omar, S. (2022). Characterization of the Ottoman ceramic tiles in the façade of Mustafa Sinan's sapil (Cairo, Egypt). *Scientific Culture*, *8*(2).

Osticioli, I., Agresti, J., Fornacelli, C., Memmi, I. T., & Siano, S. (2012). Potential role of LIPS elemental depth profiling in authentication studies of unglazed earthenware artifacts. *Journal of Analytical Atomic Spectrometry*, *27*(5), 827-833.

Oulmakki, O., Rodrigue, J. P., Hernandez Meza, A., & Verny, J. (2023). The implications of Chinese investments on Mediterranean trade and maritime hubs. *Journal of Shipping and Trade*, *8*(1), 28.

Palanivel, R., & Rajesh Kumar, U. (2011). The mineralogical and fabric analysis of ancient pottery artifacts. *Cerâmica*, *57*, 56-62.

Panagopoulou, A., Lampakis, D., Christophilos, D., Beltsios, K., & Ganetsos, T. (2018). Technological examination of Iznik ceramics by SEM-EDX, Raman, XRD, PLM: A case study. *Scientific Culture*, *4*(3), 27-33.

Porozova, S. E., Kul’met’eva, V. B., Gurov, A. A., & Vokhmyanin, D. S. (2013). Thermomechanical analysis as a tool for optimizing sintering regimes for ceramic materials based on zirconium dioxide. *Refractories and Industrial Ceramics*, *54*, 307-311.

Pradell, T., & Molera, J. (2020). Ceramic technology. How to characterise ceramic glazes. *Archaeological and Anthropological Sciences*, *12*(8), 189.

Prinsloo, L. C., Wood, N., Loubser, M., Verryn, S. M., & Tiley, S. (2005). Re - dating of Chinese celadon shards excavated on Mapungubwe Hill, a 13th century Iron Age site in South Africa, using Raman spectroscopy, XRF and XRD. *Journal of Raman Spectroscopy: An International Journal for Original Work in all Aspects of Raman Spectroscopy, Including Higher Order Processes, and also Brillouin and Rayleigh Scattering*, *36*(8), 806-816.

Rangkuti, N., & Fauzi, M. R. (2019). Archaeological evidence from Purwo Agung site (Karang Agung Tengah): A new perspective on Pre-Srivijayan settlement in the coastal area of South Sumatra. *Archaeological Research in Asia*, *17*, 193-203.

Rezaee, M., Khoie, S. M. M., & Liu, K. H. (2011). The role of brookite in mechanical activation of anatase-to-rutile transformation of nanocrystalline TiO 2: An XRD and Raman spectroscopy investigation. *CrystEngComm*, *13*(16), 5055-5061.

Ricci, G., Caneve, L., Pedron, D., Holesch, N., & Zendri, E. (2016). A multi-spectroscopic study for the characterization and definition of production techniques of German ceramic sherds. *Microchemical Journal*, *126*, 104-112.

Richard, D., & Rendtorff, N. M. (2019). First principles study of structural properties and electric field gradients in kaolinite. *Applied Clay Science*, *169*, 67-73.

Sciau, P., & Goudeau, P. (2015). Ceramics in art and archaeology: A review of the materials science aspects. *The European Physical Journal B*, *88*, 1-11.

Simsek, G., Colomban, P., Wong, S., Zhao, B., Rougeulle, A., & Liem, N. Q. (2015). Toward a fast non-destructive identification of pottery: The sourcing of 14th–16th century Vietnamese and Chinese ceramic shards. *Journal of cultural heritage*, *16*(2), 159-172.

Štubňa, I., Trník, A., & Vozár, L. (2009). Thermomechanical and thermodilatometric analysis of green alumina porcelain. *Ceramics International*, *35*(3), 1181-1185.

Swainson, I. P., Dove, M. T., Schmahl, W. W., & Putnis, A. (1992). Neutron powder diffraction study of the åkermanite-gehlenite solid solution series. *Physics and Chemistry of Minerals*, *19*, 185-195.

Tai, Y. S., Daly, P., Mckinnon, E. E., Parnell, A., Feener, R. M., Majewski, J., . . . Sieh, K. (2020). The impact of Ming and Qing dynasty maritime bans on trade ceramics recovered from coastal settlements in northern Sumatra, Indonesia. *Archaeological Research in Asia*, *21*, 100174.

Thompson, R. M., & Downs, R. T. (2008). The crystal structure of diopside at pressure to 10 GPa. *American Mineralogist*, *93*(1), 177-186.

Tite, M. S. (2008). Ceramic production, provenance and use—a review. *Archaeometry*, *50*(2), 216-231.

Tite, M. S., Freestone, I. C., & Wood, N. (2012). An investigation into the relationship between the raw materials used in the production of Chinese porcelain and stoneware bodies and the resulting microstructures. *Archaeometry*, *54*(1), 37-55.

Ueda, K., Miksic, J. N., Wibisono, S. C., Harkantiningsih, N., Goh, G. Y., McKinnon, E. E., & Shah, A. M. Z. (2017). Trade and consumption of fine paste ware in Southeast Asia: Petrographic and portable X-ray fluorescence analyses of ninth-to fourteenth-century earthenware. *Archaeological Research in Asia*, *11*, 58-68.

Velraj, G., Sudha, R., & Hemamalini, R. (2010). X-Ray diffraction and Tg-Dta studies of archaeological artifacts recently excavated in Salamankuppam Tamilnadu. *Recent Research in Science and Technology*, *2*(10).

Wen, J., Chen, Z., Zeng, Q., Hu, L., Wang, B., Shi, J., & Zhang, G. (2019). Multi-micro analytical studies of blue-and-white porcelain (Ming dynasty) excavated from Shuangchuan island. *Ceramics International*, *45*(10), 13362-13368.

Widjaja, E., Lim, G. H., Lim, Q., Mashadi, A. B., & Garland, M. (2011). Pure component Raman spectral reconstruction from glazed and unglazed Yuan, Ming, and Qing shards: A combined Raman microscopy and BTEM study. *Journal of Raman Spectroscopy*, *42*(3), 377-382.

Witkowski, T. H. (2016). Early history and distribution of trade ceramics in Southeast Asia. *Journal of Historical Research in Marketing*, *8*(2), 216-237.

Wu, J., Ma, H., Wood, N., Zhang, M., Qian, W., Wu, J., & Zheng, N. (2020). Early development of Jingdezhen ceramic glazes. *Archaeometry*, *62*(3), 550-562.

Wu, J., Zhang, M., Hou, T., Li, Q., & Wu, J. (2015). Analysis of the celadon of the Tang and the five Dynasties unearthed from Nan Kiln and Lantian Kiln site of Jingdezhen, China. *Ceramics International*, *41*(5), 6851-6857.

Xanthopoulou, V., Iliopoulos, I., & Liritzis, I. (2020). Characterization techniques of clays for the archaeometric study of ancient ceramics: A review. *Scientific culture*, *6*(2), 73-86.

Yan, B., Liu, S., Chastain, M. L., Yang, S., & Chen, J. (2021). A new FTIR method for estimating the firing temperature of ceramic bronze-casting moulds from early China. *Scientific Reports*, *11*(1), 3316.

Zhang, P., Liu, J., Du, H., Li, S., & Xu, R. (2010). A facile preparation of mullite [Al 2 (Al 2.8 Si 1.2) O 9.6]

nanowires by B 2 O 3-doped molten salts synthesis. *Chemical Communications*, *46*(22), 3988-3990.

Zouaoui, H., & Bouaziz, J. (2017). Physical and mechanical properties improvement of a porous clay ceramic. *Applied Clay Science*, *150*, 131-137.